Combustion in the air stream adjacent to a body flying at supersonic speeds produces forces on the body, because the heated air layer acts as a volume source to deflect neighboring air layers. Net thrust can be produced by external burning near rearward facing surfaces of appropriately shaped bodies or wings. Both experimental and analytical results show that "external burning ramjets" could be used for hypersonic cruise (or simply for drag reduction) but are unattractive for primary propulsion systems that must provide a significant acceleration capability. However, substantial forces normal to a body can be produced efficiently, so that a promising application of external burning is for steering control systems. Fuel specific impulses may be four to ten times those achievable with simple jet reaction systems.

F. S. Billig and G. L. Dugger

EXTERNAL BURNING IN SUPERSONIC STREAMS

Twenty years ago, when ramjets were just beginning to become useful devices and the theory of subsonic heat release in their burners was still being developed, a few adventurous spirits were already looking ahead to the possibility of burning in supersonic streams.[1,2] By 1951 experiments on drag reduction of supersonic projectiles by burning in the projectile's wake had been conducted by APL,[3] but this was still essentially a subsonic heat release phenomenon. In the period 1955-1960, a series of experiments at the NACA Lewis Laboratory[4,5] showed that very reactive fuels could indeed be burned in the supersonic flow fields around various body shapes. Meanwhile, at the Forest Grove "Burner Lab" of APL, the writers had undertaken to prove that an "external ramjet," i.e., burning beneath a flat-topped, triangular airfoil, could produce net thrust as well as lift at Mach 5 (approximately 3500 mph). The first burning test in 1959 was successful in this regard. The APL work and work by others on external burning have been summarized.[6]

An appreciation for what external burning can do in relation to other simple force-producing schemes can be gained by considering the external flow fields above flat plates in Fig. 1. The generation of a useful force on the plate requires deflection of the streamlines in such a manner that increased pressures are produced on chosen surface areas. In the absence of any disturbance, streamlines would simply pass over the plate with no pressure change ($p/p_0 = 1$ in the graph). The sketches show the disturbed streamline patterns caused by (a) an aerodynamic flap, (b) mass addi-

[1]B. L. Hicks, "On the Characterization of Fields of Diabatic Flow," *Quart. Appl. Math.* **VI**, No. 4, January 1949, 405–416.

[2]I. I. Pinkel and J. S. Serafini, "Graphical Method for Obtaining Flow Field in Two-Dimensional Supersonic Stream to which Heat is Added," NACA TN-2206, November 1950.

[3]W. T. Baker, T. Davis, and S. E. Mathews, "Reduction of Drag of a Projectile in a Supersonic Stream by the Combustion of Hydrogen in the Turbulent Wake," APL/JHU Report CM-673, June 4, 1951.

[4]E. A. Fletcher, R. G. Dorsch, and M. Gerstein, "Combustion of Aluminum Borohydride in a Supersonic Wind Tunnel," NACA RM-E55D07a, June 1955.

[5]E. A. Fletcher, "Early Supersonic Combustion Studies at NACA and NASA," *Eleventh Symposium (International) on Combustion*, The Combustion Institute, Pittsburgh, Pa., 1967, 729–737.

[6]F. S. Billig, "External Burning in Supersonic Streams," APL/JHU Report TG-912, May 1967.

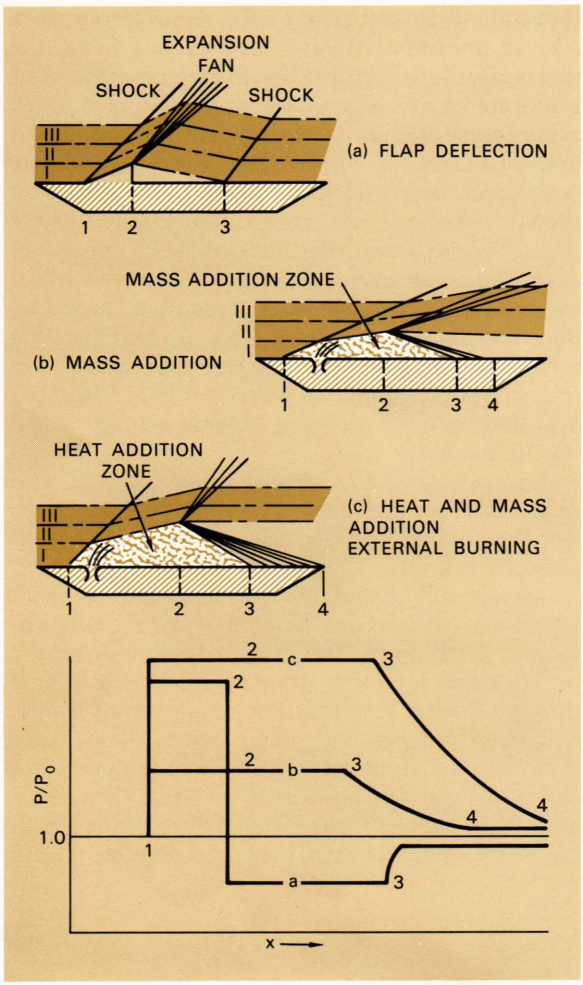

Fig. 1—Streamline patterns for various flat-plate systems in a supersonic flow, and the corresponding surface pressure profiles.

tion, and (c) mass addition plus heat addition (external burning). The corresponding surface pressure profiles are shown on the bottom portion of the figure by the lettered curves. For Case (a), the pressure rise caused by the flap must be followed by expansion to below ambient pressure at Station 2 and then recompression to about p_0 at Station 3. Thus, to obtain the greatest net positive force normal to the plate, the flap should be positioned sufficiently far aft so that Station 2 corresponds to the trailing edge of the plate. Obviously, the flap causes a drag penalty in the axial direction. For simplicity, in Cases (b) and (c) the heat and/or mass addition is confined to Streamtube I in a zone of finite length (Station 1 to Station 2) and is assumed to occur at constant pressure. The surface pressure is sustained, however, until the first expansion wave strikes the surface at Station 3, then the pressure declines to a value near p_0 at Station 4. In effect, the heat addition (and the mass addition to a lesser degree) represents a volume source in Streamtube I giving a pressure rise that turns adjacent streamtubes (II, III, etc.); this is similar to the case of the flap but with a significantly lesser expansion effect and no drag penalty. In addition to the pressure force there is a reaction force caused by injection, which has components in the thrust and/or lateral directions, depending on the angle of injection.

This crude description of the effects of the heat and mass addition zones is oversimplified, because the zones need not be at constant pressure, and the details of boundary layers and possible attendant separated zones have been omitted. However, from sketch (c) it is apparent that to obtain the greatest total normal force from the positive pressure field developed by the external burning case, it is necessary to extend the surface to the end of the expansion zone (Station 4). On the other hand, a higher force coefficient [force/(dynamic pressure x area)] would be obtained if the plate were cut off at Station 3.

Figure 2 shows three classes of possible applications of external burning: (a) side-force generating devices for attitude control, (b) thrust-generating (or drag-reducing) devices, and (c) devices that produce both thrust and attitude control (or lift). The attitude controller for an axisymmetric vehicle (Fig. 2(a)) has injection aft of the center-of-gravity (c.g.) in any one of four quadrants. Longitudinal "fences" separate the quadrants to reduce the dissipation of the positive pressure field through circumferential spillover. Note that the downward force due to external burning would cause the nose to pitch up to a positive angle of attack (α). Thus, the external burning region would be on the leeward side of the body, where, at large α, the conditions for combustion would be very poor (low pressure and temperature in an expanded flow field). However, if the external burning were being used solely to trim the body, then one might design an aerodynamically unstable vehicle, so that the external burning could be applied in a windward zone. Attitude control systems based on external burning ahead of the c.g. are conceivable but appear to be less attractive because of the difficulty of confining the positive pressure field to produce an effective pitching moment. Figure 2(b) represents either a complete vehicle or a podded or airfoil engine designed to produce thrust. At the "knee," fuel is added to the air, which has been compressed by an oblique shock and/or isentropic turning on the forebody, and combustion maintains a positive pressure field on the aft body which is greater than that on the compression surface, thus producing net thrust. Both axisymmetric and

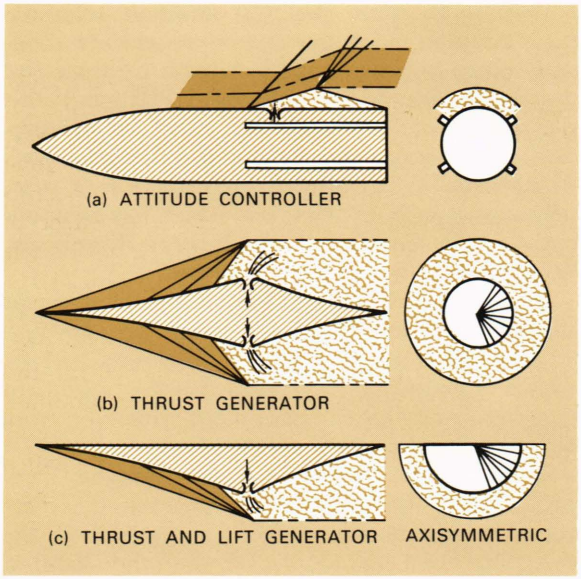

Fig. 2—External burning configurations.

two-dimensional configurations are possible for this case and for the combined thrust and lift case of Fig. 2(c). The latter, which has a flat top (hence no positive pressure on top) but a positive pressure field over its entire lower surface, develops considerable lift. It could be used as a "propulsive wing" or "external burning ramjet (ERJ)."

Testing of External Ramjets

As previously noted, experimental work at APL began with the testing of simple wedge-type ERJ's in a Mach 5 wind tunnel. When TEA, triethyl aluminum, a pyrophoric fuel (a very reactive fuel that will burn spontaneously in air at normal conditions) was injected from a lateral row of ports just ahead of the model's "knee" (see Fig. 3), combustion occurred under the rearward facing surface, as in Fig. 2(c). With no fuel injection, the air flow expanded around the knee, producing the low pressure trace (curve with circles in Fig. 3). Injection of a small amount of fuel raised the rear surface pressure (inverted triangles) almost to the level of the front surface pressure. The pressures increased as the fuel injection rate was increased, but not in direct proportion. Thus, a diminishing return effect sets in; to put it another way, an efficient ERJ is a small perturbation device. Larger fuel flows tend to be wasteful; appreciable net thrusts, as one might desire for acceleration, can not be produced efficiently, as we shall also show later by a theoretical treatment.

Figure 4 is a combined schlieren/direct-luminosity photograph from a larger scale test at the Ordnance Aerophysics Laboratory (OAL). Here the model is inverted, and its nose projects into a 32-inch-diameter, Mach 5 free-jet nozzle at the right edge of the picture. The model has a 10° front wedge and a 20° rear wedge and is 3 inches thick at the knee. Several interesting features are shown in this picture. The upper white line is the oblique bow shock from the front wedge. An "injection shock" originates just ahead of the knee, where the fuel was injected. The fuel produced a gray fog. A small amount burned upstream near the surface in a region of boundary layer separation caused by injection-shock interaction. The air and fuel fog underwent some expansion before appreciable heat release from the flame occurred. After substantial heat had been released the volume source caused the "flame shock."

A great variety of models was tested at APL and OAL—rear wedge angles of 10°, 20°, and 30°; detachable sideplates or fences to prevent spillover; detachable, horizontal, and aft extension plates that might simulate a wing surface beneath which the wedge was attached; and diamond-shaped "fuel injection pylons" extending from the wedge knee into the stream to distribute fuel through the full region of flow compressed by the bow shock (and further compressed by the pylons).

In the smaller model tests at APL, temperatures and pressures were simulated for Mach 5 flight at altitudes from 82,000 to 105,000 feet. When an aft plate extension was used, pressures on it were gen-

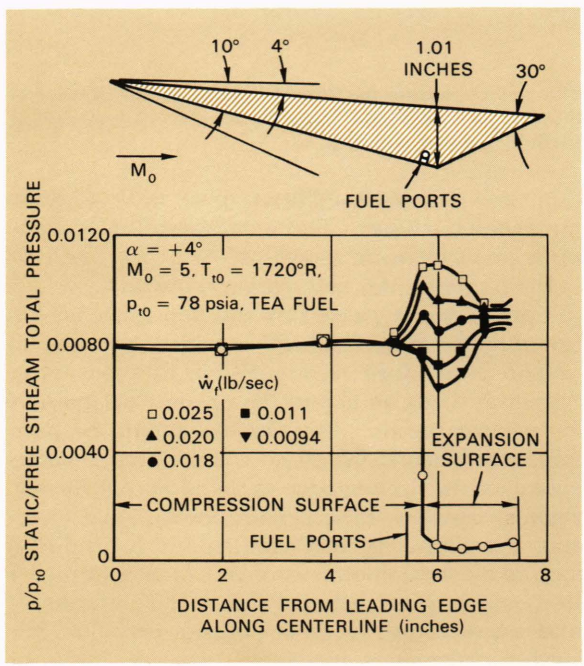

Fig. 3—Experimental pressure profiles for APL ERJ model.

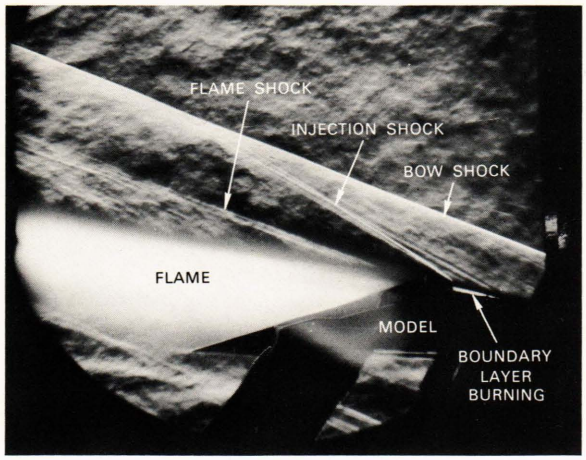

Fig. 4—Schlieren photograph from an OAL test of basic wedge model.

erally about the same as on the rearward facing wedge, indicating that heat release was still occurring downstream from the wedge. This pressure increase would increase lift at all angles of attack but would subtract from thrust for positive values of α and add for negative values. Residence time based on the air velocity was about 25 μsec in the aft wedge zone and an additional 60 μsec in the extension plate zone. Results from the other models tested were similar, with most heat release efficiencies between 25 and 60% and a few very lean operating points having about the theoretical efficiency.

In the larger scale tests at OAL, the maximum air total temperature that could be provided by the facility was 1500°R ($\sim$700°R below that required to simulate Mach 5.0 flight), hence the free-stream static temperature was $\sim$250°R, or about 140°R low, and some reservation is needed in comparing the effects in the APL and OAL tests. However, some of the effects noted were:

1. For the same ratio of fuel flow to air total pressure, results were better at a total pressure of 100 psia than at 70, 160, or 200 psia. (Corresponding pressure altitudes are 87, 82, 97, and 105 thousand feet, respectively.) If jet penetration depends primarily on the relative fuel-air momentum, then the penetration of an incompressible liquid into a compressible gas will increase with increasing air pressure for constant fuel port area and ratio of fuel flow to air pressure; e.g., doubling both the fuel rate and the air pressure quadruples the fuel momentum but only doubles the air momentum. Since the fuel penetration increases, local effective fuel-air equivalence ratios (ER's) decrease. It is conjectured that for this model and these test conditions, the most favorable ER distributions occurred with the 100 psia air total pressure.

2. The pressure level on the aft extension plate remained essentially constant and equal to that on the rear wedge, indicating that heat release was continuing. (Even though the heat release zone might effectively end, say, midway with respect to the length of the extension plate, the effect of expansion in the supersonic flow might not be felt until considerably later, as in Case (c) of Fig. 1.)

3. Results with the pylons were disappointing in that only slightly higher pressure fields were produced than without pylons. Injection from the pylons only was more effective than combined injection from pylons and body.

4. In general, the tests at OAL showed smaller thrust and lift gains per pound of injected fuel than the smaller-scale tests at APL. Besides the aforementioned lower temperature of the OAL tests, it was suggested that a dissimilar (cooler and relatively thinner) boundary layer and relative fuel jet penetration may have contributed to the scaling effects.

Theoretical Performance of ERJ's

Since the foregoing tests showed that pressures usually were nearly constant on the rear wedge, an analytical model for constant-pressure heat release following an oblique shock was developed.* (The special case of heat addition only sufficient to reduce the expansion around the knee, with no shock, also is treated by Billig,[6] but these cases always represent net drag on the vehicle.) The analysis is based on inviscid two-dimensional flow of real gases in thermodynamic equilibrium. It is assumed that the maximum amount of air that can be used in the combustion is represented by the full amount captured by the shock at the model knee. The fuel is injected and distributed through this air layer just behind the flame shock. The static pressure and the velocity component in the emergent fuel jet are matched to the air static pressure and air velocity at the injection station. Then the conservation equations (for mass, momentum, and energy) are solved in conjunction with the postulated geometry of the model and the assumption that constant-pressure heat release occurs from the injection station (and behind the oblique injection shock) to the trailing edge of the model. With these relations we obtain the fuel flow rate $\dot{w}_f$, and can calculate lift L, thrust F, and a range

*Many models for other modes of heat addition, particularly "planar heaters" either normal to or oblique to the flow, had been studied by various investigators,[6] but none was as practical a representation of the experimental evidence here (or for other feasible hardware geometries) as this constant-pressure model.

parameter, $\mathcal{K} = V_0 L/\dot{w}_f$.[†] Maximum theoretical performance is obtained when the front wedge angle δ_1 is minimum, but for practical structural considerations, δ_1 was limited to a minimum of 5°.

Figure 5 compares theoretical performance of the ERJ with that of a conventional ramjet with subsonic internal combustion (CRJ), and it shows the sensitivity of $\mathcal{K}$ to the required thrust level. For the ERJ the aft wedge angle is varied to produce maximum $\mathcal{K}$. At Mach 9 the aft wedge angle is 5° for $C_F = 0$, where $\mathcal{K}$ is 5300 n.mi.; 15° for $C_T = 0$, where $\mathcal{K}$ is 3500 n.mi; and 25° for $C_T = 0.1$, where $\mathcal{K}$ has fallen to 1500 n.mi. The CRJ curve is based on engines with inlet (kinetic energy), combustion, and nozzle efficiencies of 0.92, 0.95, and 0.96, respectively, and on vehicles with overall lift/drag ratios of 6. (The CRJ exhaust flow properties were estimated from a thermodynamic model that approximates chemical kinetic effects; on a comparable basis, the ERJ results are based on chemical equilibrium for the constant-pressure combustion under the rear wedge, and no subsequent expansion is assumed to occur.) The drastic reduction in $\mathcal{K}$ when net thrust ($C_T = 0.1$) is required suggests that the ERJ would not be attractive for high thrust or accelerating missions. Comparison of the $C_T = 0$ curve with the CRJ curve shows that ERJ's should be superior to CRJ's in cruise applications at $M_0 \geq 9$.

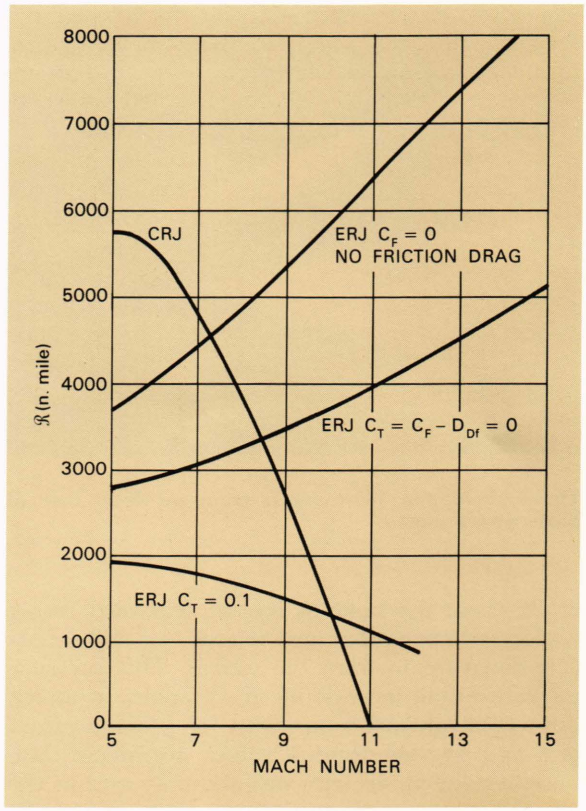

Fig. 5—Comparison of wedge-type ERJ's with various thrust requirements with CRJ vehicles with overall $L/D = 6$. All engines cruise with kerosene fuel at optimum ER.

External Burning for Attitude Control

Since we have shown that an ERJ could be an excellent cruise (or "sustainer") engine for hypersonic speeds but would not have the acceleration capability usually required of a primary propulsion device, let us turn to experiments more directly related to the production of lift (or side force) on a vehicle for attitude control. It was, in fact, the next set of experiments and related theoretical treatments at APL[7] that conclusively demonstrated, by extensive in-stream measurements, the fact that supersonic heat release was being achieved, as well as clarifying the basic features of the injection/shock-wave/boundary-layer interactions, the mechanism by which fuel droplets are carried away from the wall, and the potentials for producing side forces.

These tests were done with a water-cooled flat-plate model (Fig. 6) in a 10-in.-diam, Mach 5.0 tunnel at a simulated altitude of 66,000 ft. Fuel was injected from the most forward fuel manifold which contained twelve 0.031-in.-diam, equally-spaced fuel ports. The free-stream static pressure was 0.78 psia, and the static temperature was 355°R, (which is 35°R low for true simulation at 66,000 ft). Figure 6(b) shows static pressure profiles taken along the model centerline for "cold" flow (no injection) and for toluene and TEA injection from the forward fuel manifold. For toluene, the rather abrupt pressure rise at a point 2.5 in. from the leading edge, followed by a decay back to about the free-stream level, is as expected for nonreacting liquid injection. With TEA, the pressure first rises, then decays slightly because of the injection shock followed by weak expansion waves, and then rises to a near constant value as the heat release begins. The continuing relatively constant pressure plateau to the trailing edge indicates that heat release was continuing and had not been completed in the 12-in. length.

In order to appraise the latter situation, a study of droplet evaporation and diffusion into a second medium was undertaken. An analysis[8] which con-

[†]The Breguet cruise range (n. mi.) would be found by multiplying R by $ln(W_0/W_B)$. This logarithmic term is unity when the burnout weight W_B is 36.8% of the initial stage weight W_0; i.e., the fuel weight is 63.2%.

[7]F. S. Billig, "A Study of Combustion in Supersonic Streams," APL/JHU Bumblebee Report 321, July 1964.

[8]E. E. Zwick, D. H. Grubman, and L. Hardy, "Analysis of Droplet Evaporation and Combustion in Hypersonic Streams," Paper presented at AIAA Aerospace Sciences Meeting, January 1964.

siders spherical particles with known drag and heat transfer coefficients was used to determine the droplet diameter as a function of time, beginning with an initial droplet diameter d_0 determined by an empirical relationship.[9] For the TEA flow rate of Fig. 6, the calculated d_0 is about 9 microns. Diffusion coefficients of TEA into air were calculated using a rigid sphere model[10] based on estimated molecular diameters for TEA. As a reference, the droplet trajectory analysis by Zwick, et al.,[8] in which it is assumed that the incoming air flow remains essentially parallel to the plate, was used to compute Curve E in Fig. 7(a). It was apparent that, to account for the observed phenomena, their analysis would have to be modified to show a mechanism for greater fuel penetration.

Our experiments had shown that a separated flow zone was caused by the fuel injection and the resulting injection shock (Fig. 7(b)). We postulate that the fuel penetrates through the separated region with no effective downstream displacement

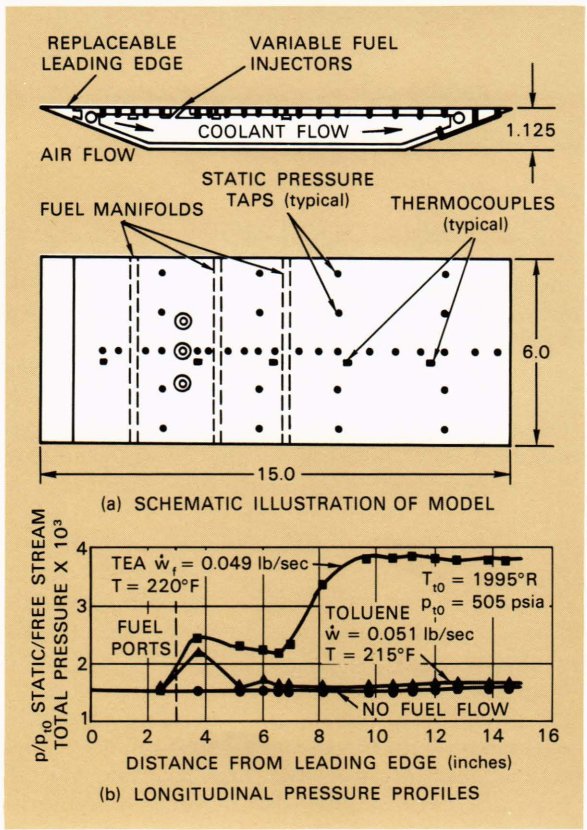

Fig. 6—Flat-plate combustor model tested at Mach 5.

[9]R. Ingebo, and H. Foster, "Drop Size Distribution for Cross-Current Break-up of Liquid in Airstreams," NASA TN-4087, October 1957.

[10]J. O. Hirschfelder, C. F. Curtiss, and R. B. Bird, *Molecular Theory of Gases and Liquids*, John Wiley and Sons, Inc., New York, 1954.

and then encounters an airstream that is moving not parallel to the plate, but away from it at an angle determined by the injection-separation shock strength. Thus, the air stream accelerates the droplet both downstream and away from the plate. Subsequent turning of the air stream owing to expansion and then recompression by the flame shock similarly affects the droplet. Downstream from the flame shock the streamline directions vary with distance from the plate, according to the postulated constant-pressure heat addition model. A streamline near the plate remains parallel to it, but one farther outboard follows the theoretical deflection angle for the injection shock. The droplet trajectory Curve D in Fig. 7(a) represents the latter case, whereas Curve C represents a droplet that travels well into the heat-addition zone. These curves accordingly diverge 4.75 in. from the injection point where they first encounter the flame zone. For reference, the wavy line A represents the approximate boundary of the observable luminous zone and point B represents a point on the boundary of heat release as deduced from pitot-pressure measurements.

Further analyses were based on the model in Fig. 7(b), in which the incoming air is divided into three major streamtubes: boundary layer air, inviscid burned air, and air that is turned but not burned. The height h_1 of the boundary layer streamtube reaching the injection shock is determined by a cold-flow pitot-pressure traverse and checked with a calculated boundary-layer thickness. After fuel injection it is assumed that no further flow into the boundary layer occurs and that the height h_4 exceeds h_1 because of heat release and additional viscous losses. The downstream pitot traverse determines h_6 and the sum of h_5 and h_4. Since the flow in the outside streamtube (h_6) is inviscid and adiabatic, the upstream height h_3 can be specified by solving wedge-flow relationships consistent with observed shock waves and pressure measurements. Now knowing h_1 and h_3, and knowing that $h_1 + h_2 + h_3 = h_4 + h_5 + h_6$, we can determine h_2 by difference. We assume that the injected fuel is divided between Streamtubes I and II in proportion to the air flows entering them. The only remaining items needed to analyze the combustion are the $\int pdA$ terms in the momentum equation for the three streamtubes. For each streamtube this integral is the product of the local pressure and the incremental projected area in the flow direction summed over the streamtube boundaries.

For the test of Fig. 6(b), the pitot profile measurements at the traversing plane, which was 7.3 in. downstream from the port, showed $h_5 + h_4 = 1.20$ in. The calculated values for h_1, h_2 and h_3 were

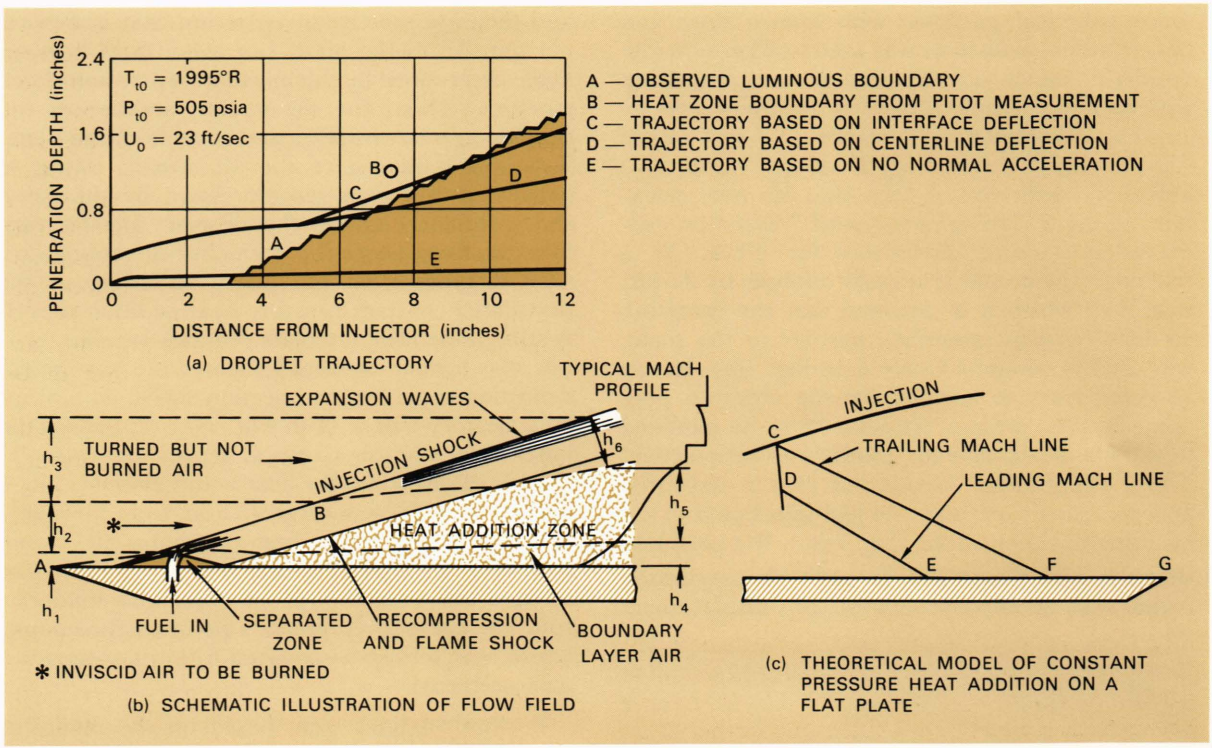

Fig. 7—Schematic illustration of flat-plate combustor flow field and calculated droplet trajectories.

0.05, 0.61, and 1.93 in., respectively. The average ER in the combustion zone was near 1.0, and the calculated average combustion efficiency (η_c) at the traversing plane was only 31.5%. Now, if we postulate that additional plate length is available (see Fig. 7(c)), and that heat release would continue at the same average rate (at the same pressure), combustion would be completed at point D, 24 in. from the leading edge. Moreover, the pressure in this flame zone is well above ambient, and further force can be realized by using a still longer plate to account for expansion of both the burned gas and the air compressed in Streamtube III. Expansion begins in the combustion gas at point D, as represented by the "leading Mach line," DE. No change in pressure on the surface will be felt before this Mach line strikes it. Pressure is therefore assumed to be constant throughout the region ABDE (refer to Fig. 7(b) for points A and B). For our test, the length $\overline{AE}$ would be 31 in. At point C, the air will also begin to expand (Mach line CF). For simplicity we assume that the average pressure from E to F is the arithmetic mean of our combustion pressure p_{AE} and the free-stream pressure p_0; i.e., $p_{EF} = (p_{AE} + p_0)/2$. Using these pressures, the normal force produced per unit model width d is

$$N/d = (p_{AE}\overline{AE} + p_{EF}\overline{EF}) - p_0(\overline{AE} + \overline{EF}),$$

and the normal-force fuel specific impulse for our test is $I_{fN} = N/\dot{w}_f = 5760$ sec. (In contrast, the I_{fN} measured by integrating the pressure rise over the available 12-in. length for the test model was 1350 sec.)

From the theoretical constant-pressure heat addition model it is also possible to determine the variation of total temperature (hence Mach number) with distance in the constant-pressure heat release zone for a given capture height, $h_1 + h_2$. Thus, in tests (including the Fig. 6 test) made at nearly the same condition, extensive pitot pressure surveys were made and local Mach numbers were deduced. In Fig. 8 these values are compared with curves from the theoretical analysis. The abscissa in the figure is the distance along the streamline from the point of first perceptible heat release to the pitot measuring station. The close correlation of the data with the theory suggests that the theoretical description of the heat release, viz, the prescribed continuous rise in total temperature with distance, is reasonable for these tests.

Summary Comparisons of External Burning Data from Various Sources

The realization of the potentials of external burning depends on obtaining high combustion efficiency in short distances and on developing

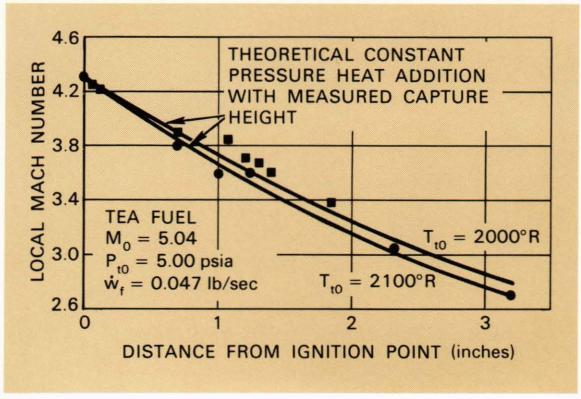

Fig. 8—Mach number as a function of distance from ignition on a flat-plate combustor.

the desired pressure coefficients. Figure 9 shows the degrees to which these goals have been obtained in experiments by various organizations. Figure 9(a) shows I_{fN} versus M_0 and includes theoretical curves for the two fuels tested based on the constant-pressure combustion analysis including expansion (Figs. 7(b) and (c)).[6] The difference between the curves in Fig. 9(a) is due to the different heating values of the fuels: 23,390 Btu/lb for aluminum borohydride ($Al(BH_4)_3$ and 18,360 Btu/lb for TEA. Data points with bar extensions, D through H, represent the ranges of values obtained in several tests of the same model.

For nearly all of the data in Fig. 9(a), the length available for combustion was small and/or the static temperatures were lower than for simulated flight; therefore, the specific impulses are lower than the corresponding theoretical values. The early NASA tests (points A through C) show the best results, probably because (a) $Al(BH_4)_3$ fuel is more reactive, (b) the static pressure in test A was the highest of all cases, and (c) the models used in B and C were relatively long. Case E from APL tests of a small wedge model gave better results than cases G and H for larger models tested at OAL, probably because the air temperatures were lower at OAL. However, between cases G and H the beneficial effect of greater length is seen.

Nearly all of the points have I_{fN} values considerably in excess of the values that can be obtained with nonreactive attitude-control systems. The performance of a cone, $\mathcal{J}$, was poorer than for the two-dimensional models, apparently because of excessive spillover of the pressure field around the body. This result points to the desirability of using longitudinal fences (such as were sketched in Fig. 2(a)). Thrust specific impulses were calculated[6] for most of the thrust-generating configurations and are low compared to either theory or competitive propulsion systems. The highest value of 818 sec for test E was obtained at the very low fuel flow rate of 0.0025 lb/sec. Although for many of the tests it could be argued that nonoptimum fuel injection systems produced poor fuel-air distributions, and performance suffered accordingly, it is likely that the limiting factor was insufficiently rapid kinetic rates; i.e., for the local conditions there was not sufficient time (distance) to complete the heat release. This argument is supported by in-stream measurements which were discussed in connection with Fig. 7. Lengths of the order of 2 or 3 feet apparently are required if theoretical impulse values are to be realized.

The other performance characteristics, especially important in the case of the attitude controller, are the normal force coefficient C_N and the pressure coefficient C_p. In most cases, it is desirable to have maximum C_N, which, at first glance, would seem to be associated with an external burner that creates a very strong shock, possibly a normal shock. However, this flow situation cannot exist, because at pressure ratios considerably below the normal-shock value, the boundary layer will separate ahead of the heat release zone, and the resulting C_p due to the volume source created by the heat release will be more like that of a separated flow. In Fig. 9(b), maximum local C_p [$C_{p_{max}} = (p_{max} - p_0)/q_0$], where q_0 is the free-stream dynamic pressure, occurring anywhere in the combustion zone for a given test, is shown as an open symbol, and the corresponding C_N for the heat addition region is shown as a closed symbol. Two theoretical curves are shown. The upper one is based on deflecting the air stream by 15°, which might represent a reasonable upper bound for theoretical system studies. The lower theoretical curve corresponds to the pressure ratio required to separate a turbulent boundary layer.

Most of the $C_{p_{max}}$ points in Fig. 9(b) data fall near the curve for turbulent boundary layer separation.[6] Some of the data were obtained at low Reynolds numbers where the boundary layer should have been laminar, which probably accounts for the lower $C_{p_{max}}$ values, because laminar separation occurs at lower C_p. Even in the NASA tests, A through C, in which the pressure distribution due to injection and heat release was characterized by a pressure spike followed by a rapid decay, the maximum pressure coefficients in the spike region still were of the same order as the turbulent separation value.

It appears that the designer of an external-burning system for attitude control will have to contend with relatively low C_p's, probably close to the separation values for the local condition at injection, and correspondingly low C_N's. If higher force

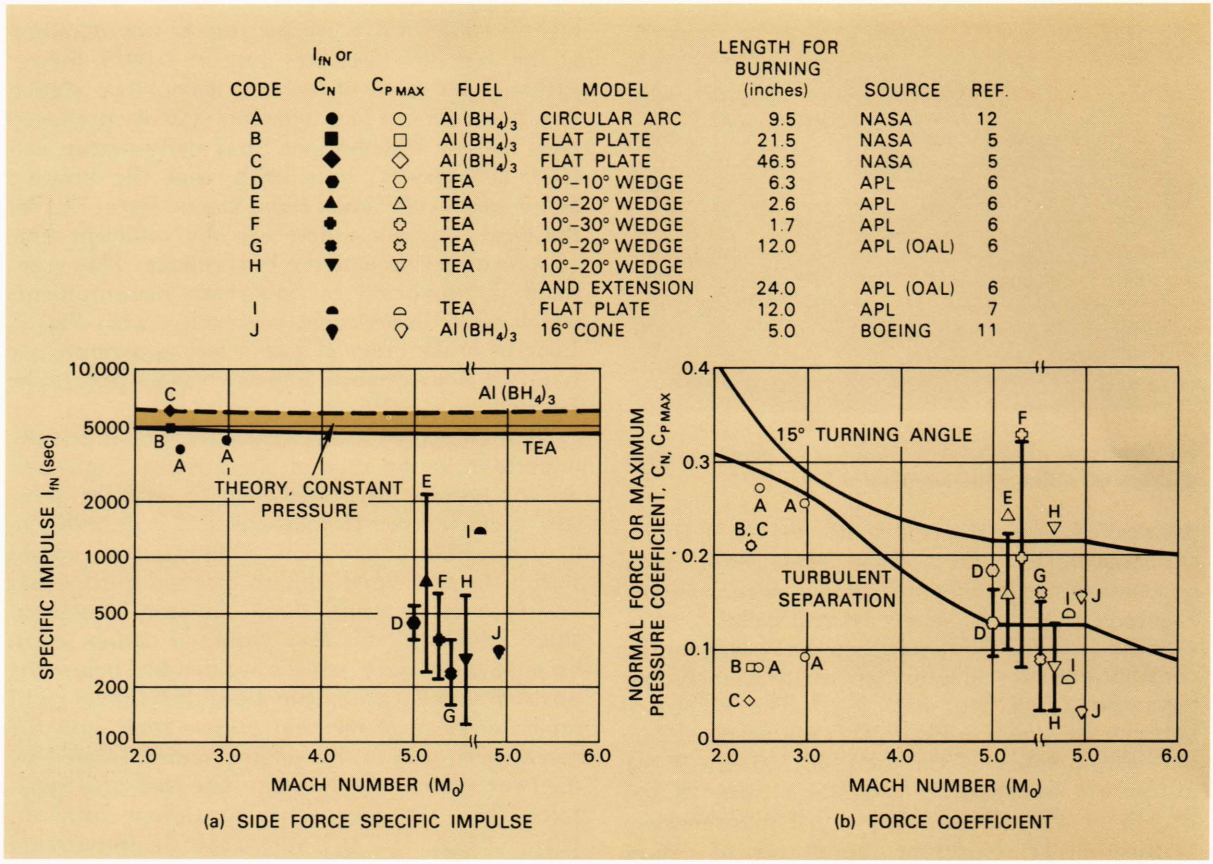

Fig. 9—Summary of experimental results.

coefficients are required, a combination of a compression surface plus external burning will be needed.

Summary and Conclusions

Extensive testing and analysis has indicated that external burning ramjets could be used for cruise propulsion at hypersonic speeds. They are very simple, and combustion heating problems would be minor since the entire "engine" could radiate to the atmosphere. The external burning principle could also be used for drag reduction of various vehicles, or under-wing burning could augment the effective L/D of an aircraft. However, it appears doubtful that an ERJ would be chosen as a primary propulsion device because it could not efficiently provide any appreciable acceleration capability. A more promising area appears to be normal-force production for attitude control of hypersonic vehicles. Here the designer probably will have to contend with pressure coefficients close to the values that would result from turbulent boundary layer separation at the point of injection, as well as correspondingly low normal force coefficients. If higher force coefficients are needed, a compression surface probably would have to be added.

If our discussion of external burning has stirred your imagination, you may wish to dig into the theory of[13,14] and potentialities for supersonic burning in ducted flows,[15-17] the basis for "scramjets."

---

[11]P. G. Kranz, and D. A. Pelky, "Experimental Investigation of External Burning on an 8° Half-Angle Cone at Mach 5.0 and 6.1," The Boeing Company, No. D2-36037, August 1964.

[12]J. S. Serafini, R. G. Dorsch, and E. A. Fletcher, "Exploratory Investigation of Static- and Base-Pressure Increases Resulting from Combustion of Aluminum Borohydride Adjacent to Body of Revolution in Supersonic Wind Tunnel," NACA RM-E57E15, October 1957.

[13]F. S. Billig, "Design of Supersonic Combustors Based on Pressure-Area Fields," *Eleventh Symposium (International) on Combustion*, The Combustion Institute, Pittsburgh, Pa., 1967, 755–769.

[14]F. S. Billig, R. C. Orth, and M. Lasky, "Effects of Thermal Compression on the Performance Estimates of Hypersonic Ramjets," *J. Spacecraft Rockets* **5**, No. 9, September 1968, 1076–1081.

[15]G. L. Dugger, "Comparison of Hypersonic Ramjet Engines with Subsonic and Supersonic Combustion," *Combustion and Propulsion, Fourth AGARD Colloquium*, A. L. Jaumotte, A. H. Lefebvre, and A. M. Rothrock, Editors, Pergamon Press, New York, 1961, 84–119.

[16]W. H. Avery, "Beyond the Supersonic Transport," *Sci. & Technol.* No. 74, February 1968, 40–43, 46–50.

[17]A. Ferri, "Review of SCRAMJET Propulsion Technology," *J. Aircraft* **5**, No. 1, January-February 1968, 3–10.